Haverford College

Haverford Scholarship

Probability distributions and thermal transport in a turbulent grid flow

B. R. Lane

O. N. Mesquita

S. R. Meyers

Jerry P. Gollub
Haverford College

Repository Citation

Lane, B. R., et al. "Probability distributions and thermal transport in a turbulent grid flow." Physics of Fluids A: Fluid Dynamics (1989-1993) 5.9 (1993): 2255-2263.

Probability distributions and thermal transport in a turbulent grid flow

B. R. Lane, O. N. Mesquita, S. R. Meyers, and J. P. Gollub

Additional information on Phys. Fluids A

Probability distributions and thermal transport in a turbulent grid flow

B. R. Lane, O. N. Mesquita,[a) S. R. Meyers, and J. P. Gollub[b)
Department of Physics, Haverford College, Haverford, Pennsylvania 19041, and Department of Physics,
University of Pennsylvania, Philadelphia, Pennsylvania 19104

Recent theoretical proposals concerning non-Gaussian statistics of passive scalars in random velocity fields are tested experimentally, by measuring the probability distributions of fluctuating temperature in an oscillating grid flow across which a steady temperature gradient is maintained. Pronounced exponential tails occur at sufficiently high Reynolds number R, and predominantly Gaussian statistics at low R. When the extended tails are present for the passive scalar, the corresponding velocity power spectrum shows reasonable scaling, and the velocity distribution is not far from Gaussian. The present paper provides a more complete characterization of the flow field than an earlier brief report [Phys. Rev. Lett. 67, 3507 (1991)], and also contains a description of additional features, such as the skewness of the distributions. Finally, the effective or eddy diffusivity of both heat and a molecular impurity are measured and compared.

I. INTRODUCTION AND BACKGROUND

Turbulent flows can enhance the mixing of passive scalars such as heat and impurities by many orders of magnitude, a process that is often described by the phenomenological concept of *eddy diffusion*. The dependence of this process on the statistical properties of the flow is a difficult problem mathematically, because the large scales relevant to bulk transport are affected by a wide range of smaller scales.[1] Yet the phenomenon itself is widespread in turbulent flows, and is particularly important in geophysical flows.

In attempting to characterize turbulent mixing, it is natural to focus on the statistics of the *fluctuations* of scalar quantities, and especially on their probability distribution functions (pdf's).[2,3] The present experimental investigation was designed primarily to explore the statistics of passive temperature fluctuations in the presence of an imposed steady mean gradient, especially the deviations from Gaussian behavior. Secondarily, we study the effective or eddy diffusivity as a function of Reynolds number, for both heat and a molecular impurity.

The observation of exponential pdf's of the local temperature in turbulent Rayleigh–Bénard convection[4–6] attracted attention to the statistics of passive scalar fluctuations in turbulence. It has long been recognized[7–10] that the statistics of local velocity and temperature *derivatives* can be non-Gaussian, a phenomenon that is related to small-scale intermittency. On the other hand, the statistics of the passive scalar fields themselves were thought to be Gaussian before the experiments on thermal turbulence.

Subsequently, Pumir *et al.*[11] proposed a simplified model of random advection for situations in which a steady mean gradient is maintained across the flow. Their one-dimensional phenomenological model yielded exponential tails, which arise basically from instances in which fluid at a given location comes from distant locations where the local mean value is systematically larger or smaller. The significance of these distributions, which are broader than Gaussians, is the implication that fluid can be transported over long distances without mixing.

Several numerical investigations have also provided support for the existence of non-Gaussian fluctuations in passive scalar fields. Kerstein[12] found exponential tails in a linear eddy model in the presence of a mean gradient. In this stochastic one-dimensional simulation, the mixing is approximated by a sequence of independent instantaneous rearrangement events followed by deterministic diffusion. This model has been extended to two dimensions by Holtzer and Pumir,[13] and these authors also showed that the model of Ref. 11 can be derived heuristically using Kerstein's approach.

Simulations in which there is no mean gradient have been conducted by several groups. Métais and Lesieur used large eddy spectral methods[14] and noted transient exponential tails. Eswaran and Pope[15] performed a direct simulation of the time evolution of the pdf starting with delta functions, and found Gaussian behavior. Finally, Ching and Tu[16] studied passive advection by a random incompressible Gaussian velocity field on a two-dimensional square lattice. They found that the steady-state pdf could take various forms (Gaussian, exponential, or stretched-exponential) depending on the parameter $C = \xi^2 / \tilde{D}\tau$, where ξ and τ are the correlation length and time, and $\tilde{D}$ is a renormalized or eddy diffusivity at the scale ξ. This parameter is generally of order 1 for turbulent flows. The results of this simulation were similar *with or without* a mean gradient.

Sinai and Yakhot[17] showed that the pdf for a random velocity field can be expressed in terms of the conditional expectation value of the normalized scalar dissipation rate (the normalized mean square spatial gradient of the scalar

field). Recently, Pope and Ching[18] pointed out that the pdf for any stationary process can be obtained exactly from conditional expectations of time derivatives of the same signal. A special case of this interesting result was pointed out by Ching.[19]

Our experiments differ from studies of temperature statistics in turbulent thermal convection, where the temperature is not passive. The experimental geometry involves a steady horizontal temperature gradient placed across a turbulent flow generated by a vertically oscillating grid. Preliminary results of this investigation were published earlier.[20] A complementary study in a wind tunnel was undertaken simultaneously by Jayesh and Warhaft,[21] and a full report of that work has appeared.[22] Interesting related measurements of pdf's for *thermally stratified* turbulence have been reported by Thoroddsen and Van Atta.[23] There have been several earlier studies of mixing phenomena that include passive scalar pdf's (e.g., Ref. 24). These have elucidated the dependence of the distributions on Reynolds number and Schmidt number in several different geometries. These earlier measurements did not focus specifically on the low probability events far from the mean.

After discussing the various experimental methods employed in this investigation, we describe the measurements of enhanced transport in Sec. III, including both thermal and mass transport in the same geometry. Section IV is devoted to a report on the statistics of temperature fluctuations, along with a more thorough characterization of the velocity field than is contained in the preliminary report.[20] Our work is compared with that of Ref. 22 and discussed in the light of theoretical studies in Sec. V.

II. EXPERIMENTAL METHODS

A. Apparatus

The mixing apparatus consists of a rectangular Plexiglas box divided into three baths, as shown in Fig. 1(a). The center bath contains the working fluid, and its interior horizontal dimensions are $L=12.5$ cm (in the direction of the gradient) by 25 cm (perpendicular to the gradient). The depth of the fluid is variable, but is generally chosen to be 7.5 cm. The temperature gradient across the working fluid is maintained by two temperature-controlled baths which are separated from the center bath by copper plates 0.3 cm thick. The control baths are stirred vigorously. One of them is controlled by fluid from a refrigerating circulator, and the other is resistively heated. The temperature difference is about 3 K, with a stability of ±0.01 K over long periods. A mean working temperature near room temperature is selected to minimize heat leaks to and from the room. The entire apparatus is thermally insulated with closed cell styrofoam about 1 in. thick, and there is no air space above the fluid.

The working fluid is mixed by an oscillating grid made by drilling a hexagonal array of holes (diameter $d=0.48$ cm; nearest neighbor spacing 0.8 cm) through a Plexiglas sheet 0.3 cm thick. The pattern of holes is shown in Fig. 1(b). The open fraction f of the grid is 0.326; larger values result in less effective mixing. The grid oscillates through
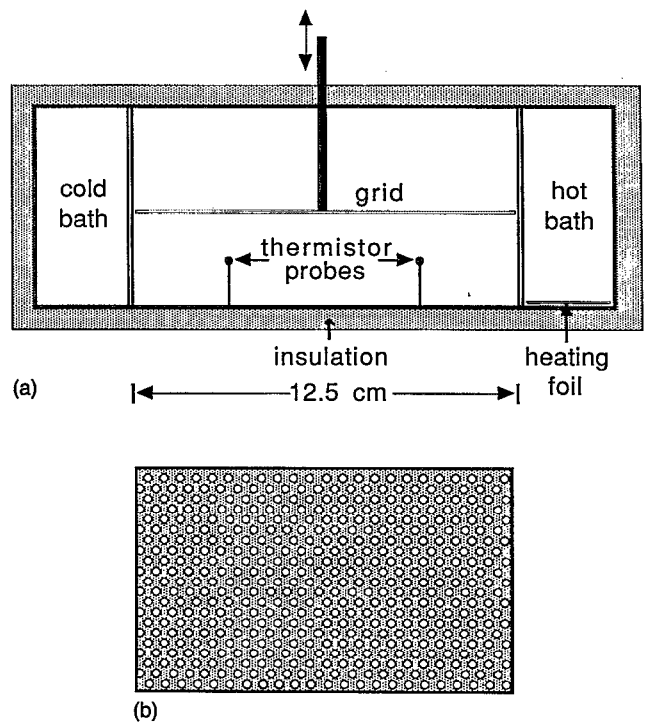

FIG. 1. (a) Sketch of the apparatus (side view), showing the oscillating grid, temperature control baths, and exterior insulation. (b) Hexagonal array of holes in the oscillating grid.

the middle 40% of the fluid depth, with periods T in the range 0.5–10 sec. We also made supplementary measurements using a different grid with holes four times as large for comparison.

Both water and water–glycerol mixtures are employed as the working fluid. The experiments are described in terms of a Reynolds number R based on the diameter d of the holes in the grid and the maximum velocity of the fluid through the holes, which depends on f. It may be expressed in terms of the period T as follows:

$$R=2\pi Ad/vTf, \tag{1}$$

where v is the kinematic viscosity and A is the amplitude of oscillation. The definition of R used in our preliminary report, Ref. 20, was higher by a factor of 2. The rms *horizontal* velocity is smaller than the maximum vertical velocity by a factor of about 0.06 at $R=3000$.

B. Temperature measurements

Temperature measurements are made using two thermistor probes of diameter 0.05 cm which have a frequency response (in a moving fluid) of about 50 Hz. Their *effective* resolution is estimated to be approximately 1 mm parallel to the local flow, which is small enough to resolve the scales of interest. The probes protrude from glass capillaries, which are in turn mounted in small Plexiglas blocks that slide in grooves milled in the bottom of the cell. The probes are located about 1.3 cm above the bottom of the cell. They can be translated independently across the cell in the direction of the temperature gradient. In this way, measurements of temperature differences and correlation func-

tions can be obtained. The effect of varying the distance from the probes to the grid is explored by varying the vertical mean position of the grid. A third probe is mounted above the grid for measurements of the vertical temperature gradient.

The probes are individually calibrated, and their resistances are fitted accurately to a quadratic function over the relevant temperature range. The resistances are sampled, typically at 10 Hz, by a Keithley 199 digital multimeter. Local heating of the probes by the measuring current is negligible, and the measurement precision is estimated to be 5×10^{-4} K.

In order to study the enhancement of heat transport by the flow, one can measure the ratio of the total flux F through the cell to the local temperature gradient β in the bulk of the fluid. This method assumes that a steady state has been achieved. It also presumes that the transport is diffusive, and that the effective diffusion coefficient D^* can be assumed uniform in the bulk of the fluid and time independent. In fact, it depends somewhat on the vertical coordinate (distance from the oscillating grid), and also must have an oscillatory component at the externally imposed frequency. So, the result is effectively averaged with respect to the vertical coordinate and time. We find D^* from the expression

$$D^* = F/\beta\rho c, \tag{2}$$

where ρ and c are the density and heat capacity of the fluid. The total flux through the fluid is determined from the power supplied to the resistive heater in the warm bath. Heat leaks to the environment are sufficiently small that corrections are not required.

C. Concentration measurements

In order to compare the *thermal* transport measurements to the transport of a diffusing *impurity*, we have also studied the spreading of fluorescein dye introduced by local injection. A laser light sheet passes through the Plexiglas cell parallel to the oscillating grid at the same vertical position as the original thermistor probes (approximately 5 mm below the lowest point of the grid). A dye solution is introduced locally in the place of the light sheet. The local dye concentration, which is linear in the scattered light intensity, can then be monitored as a function of time by digital image processing methods. The concentration field in the plane of observation is statistically isotropic. Therefore we focus attention on the azimuthally averaged field $c(r,t)$, where the origin is taken to be the location of the centroid at a given time. Two methods are used to analyze this data in order to test whether an effective diffusion model is adequate and to obtain the effective diffusion constant D_{dye}^*.

The first method focuses on the spatial distribution of the dye at a given time. Since the vertical spreading of the dye is very fast, we start with the hypothesis that the dye patterns in a horizontal plane can be described statistically by the two-dimensional diffusion equation

$$\frac{\partial c}{\partial t} = D_{dye}^* \nabla^2 c, \tag{3}$$

where D_{dye}^* is a function of the Reynolds number. The (azimuthally averaged) concentration field of a spreading spot should then vary with radius and time as

$$c(r,t) \propto \frac{1}{t} \exp\left(\frac{-r^2}{4 D_{dye}^* t}\right). \tag{4}$$

Then a plot of $\ln[tc(r,t)]$ vs $(-r^2/4t)$ will have a linear region with slope $1/D_{dye}^*$. We find it necessary to average a number of images in order to obtain reasonable linearity and adequate statistics. An alternative *time-dependent* analysis can also be used to obtain D_{dye}^*. If the time-dependent concentration field is adequately described by (3), the second moment of the radial distribution $c(r,t)$ for a spreading spot is given by

$$\langle r^2 \rangle = 2 D_{dye}^* t. \tag{5}$$

D. Local velocity measurements

Standard methods of laser Doppler velocimetry are used for local velocity measurements. The velocity component parallel to the temperature gradient is determined using a forward-scatter dual beam configuration, with resolution of 0.1 mm transverse (and approximately 1 mm parallel) to the beams. We dope the fluid with 0.4 μm polystyrene latex spheres, and utilize a Dantec 55N21 phase-locked-loop tracker for signal processing. These measurements are less precise than the thermal measurements, typically $\pm 1\%$.

III. RESULTS: TRANSPORT ENHANCEMENT

A. Temperature profiles and mean gradients

Over the full range of R explored in this investigation, most of the temperature drop occurs in the boundary layers near the copper plates separating the working fluid from the adjoining control baths. The interior temperature then varies linearly and gradually from one side to the other, as shown in Fig. 2(a). However, the mean temperature gradient in the interior varies nonlinearly with R, as shown in Fig. 2(b). The steep decline near $R = 10^3$ implies a substantial increase in bulk thermal transport over a relatively narrow interval in R. The details of this transition presumably depend on the geometry of the grid.

B. Nusselt number and effective diffusion coefficient from global measurements

The measured nondimensional total heat transport N is shown in Fig. 3(a). This quantity is simply the total heat flux through the cell, normalized by the conductive flux in the absence of fluid motion. The variation of the total flux with R is basically determined by the rate at which the boundary layers at the hot and cold vertical boundaries are thinned by the increasingly vigorous stirring. We find that N can be approximated by a power law over much of the range explored:
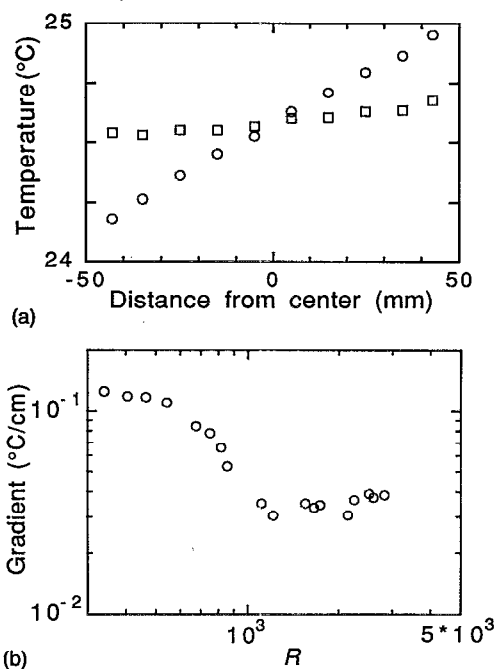
FIG. 2. (a) Mean temperature profile $\bar{T}(x)$ parallel to the temperature gradient at $R=250$ (circles) and at $R=1850$ (squares). The corresponding standard deviations of the temperature fluctuations are 0.7 K and 0.5 K, respectively, and the total temperature difference across the cell is 3 K. (b) Interior temperature *gradient* as a function of R.

$$N=0.32R^{0.64\pm0.05}. \qquad (6)$$

The boundary-layer thickness at $R=1850$ is about 1.4 mm.

We display the effective *bulk* thermal diffusion coefficient D^* as a function of R in Fig. 3(b). For comparison, note that the *molecular* thermal diffusion coefficient is $D=1.46 \times 10^{-3}$ cm^2/sec. Even for R of the order of a few hundred, the transport is dramatically 700, and then much more rapidly. At $R=2500$, the enhancement factor D^*/D is about 10^3.

Typical values of D^* are roughly consistent with Vd, where V is the root-mean-square velocity of the fluid, and d is the hole diameter. Above the transition region, D^* continues to increase gradually, perhaps linearly, but the accuracy and range of R are not sufficient to define a precise relationship.

C. Local dye transport measurements

It is of interest to compare the effective *thermal* diffusivity D^* with the effective *impurity* diffusivity D^*_{dye} obtained by following the time dependence of the second moment of a spreading dye patch, as described in Sec. II C. We find that the second moment varies approximately linearly with time once the fluctuations are reduced by suitable azimuthal and ensemble averaging. Therefore, it is not unreasonable to define an effective impurity diffusivity; its dependence on R is presented in Fig. 4. Two features are immediately evident. First, the dye transport does not show the well-defined transition region seen near $R \approx 1000$
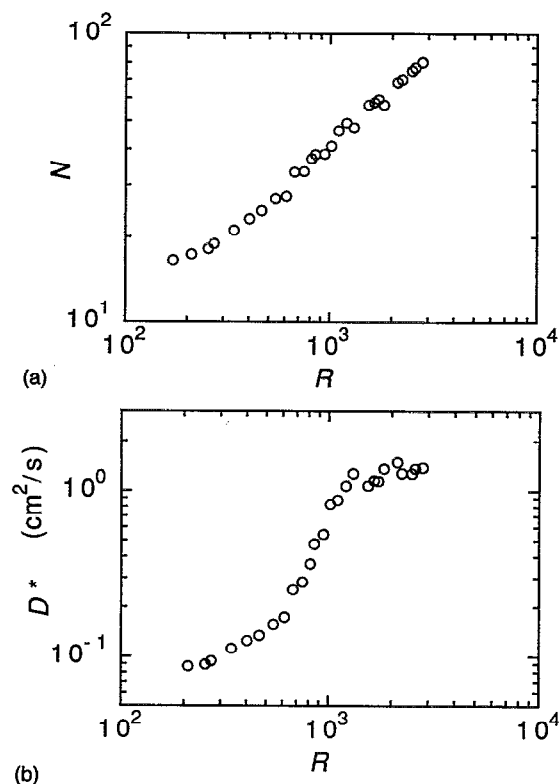

FIG. 3. (a) Nusselt number N (nondimensional heat transport) as a function of Reynolds number R. (b) Effective *thermal* diffusivity D^* defined by Eq. (2) as a function of Reynolds number.

in the bulk *thermal* transport. However, the substantial statistical fluctuations for local transport measurements lead to considerable scatter in the data. Second, the effective diffusivity of the dye is at least a factor of 10 less than the effective thermal diffusivity even at large R. For comparison, note that the ratio of the *molecular* diffusion coefficients for dye and heat is 3.4×10^{-3}. These observations suggest that the *effective* diffusivity depends on the
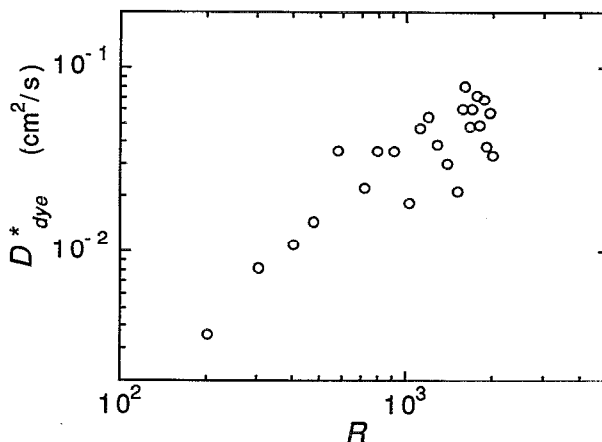

FIG. 4. Effective *impurity* diffusivity D^*_{dye} as a function of Reynolds number. The dye appears to be transported less effectively than is thermal energy.
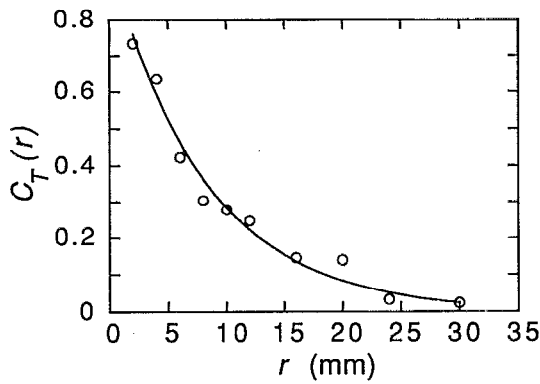
FIG. 5. Spatial correlation function of the local temperature field in the turbulent regime, showing roughly exponential decay at $R=1850$. The correlation length of 8 mm is comparable to the spacing between holes in the grid.

molecular diffusivity over the range of Reynolds numbers of our experiments, even when the fluid is turbulent.

IV. RESULTS: TEMPERATURE PROBABILITY DISTRIBUTIONS

### A. Spatial correlation function of the temperature field

In order to characterize the degree of disorder in the thermal field, we compute the spatial correlation function $C_T(r)$ of the temperature field as a function of the separation of two probes:

$$C_T(r) = \frac{\langle \delta T(r)\delta T(0) \rangle}{\langle \delta T^2 \rangle}, \quad (7)$$

where $\delta T(r)$ is the local deviation of the temperature from its long term mean value. This function is displayed in Fig. 5 for $R=1850$. It is well approximated as an exponential with a correlation length $\xi_T = 8$ mm, a value that is approximately equal to the hole spacing in the grid. The correlation function was not investigated for much lower values of R, where its structure may be more complex.

B. Characterization of the velocity field

It is important to know whether the velocity field itself is non-Gaussian, in order to be able to interpret the statistics of the thermal field. For this reason, we investigated the probability distribution functions for the component of horizontal velocity parallel to the temperature gradient. (However, it is believed to be essentially isotropic in the horizontal plane.) We find that, *for sufficiently high R (above $R \approx 1000$), the velocity pdf's are nearly Gaussian.* An example is shown in Fig. 6(a) for $R=2450$. The horizontal axis is expressed in units of the standard deviation, and the distributions are shown on a semilog scale, where a Gaussian function would be parabolic. We believe that the weak deviations from the parabolic fit on the low side could be an instrumental artifact due to imperfect locking in the laser Doppler tracking electronics. For *low R* (below 500
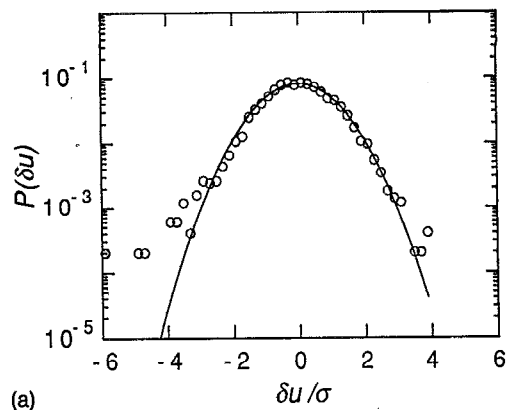
(a)
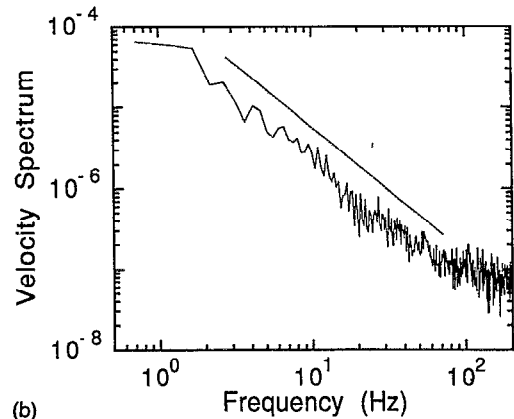
(b)

FIG. 6. (a) Probability distribution of the local velocity at $R=2450$; the solid line is a Gaussian fit to the data. The weak deviations from the fit on the low side could be an instrumental artifact. For much lower R, the velocity pdf is clearly non-Gaussian (see text). (b) Velocity power spectrum, showing a reasonably well-developed inertial range with slope close to $-5/3$ (solid line).

roughly) $P(\delta u)$ was clearly non-Gaussian, a reflection of the oscillatory nature of the forcing, which gives pulsing jets at a given location.

To confirm that the turbulence is well-developed, we also determine the local velocity spectrum, as shown in Fig. 6(b). The spectrum shows a reasonable inertial range with slope close to $(-5/3)$. (The background spectrum is essentially white, and does not influence the measurements appreciably at frequencies below about 50 Hz.) Thus, measurements of the velocity field and its distribution confirm that toward the upper end of the accessible range of R, the velocity field is in fact turbulent, though it is also anisotropic.

C. Measured temperature distributions

The central goal of this investigation was to determine the behavior of the distribution function $P(\delta T)$ for temperature fluctuations δT measured from the local mean. Our most important observation is that roughly exponential tails develop in the distributions as R is increased. This change is visible in the local temperature time series shown in Fig. 7 for $R=300$ and 1850. The temperature is expressed in units of the standard deviation. The proportion of large excursions is clearly enhanced in the second case.
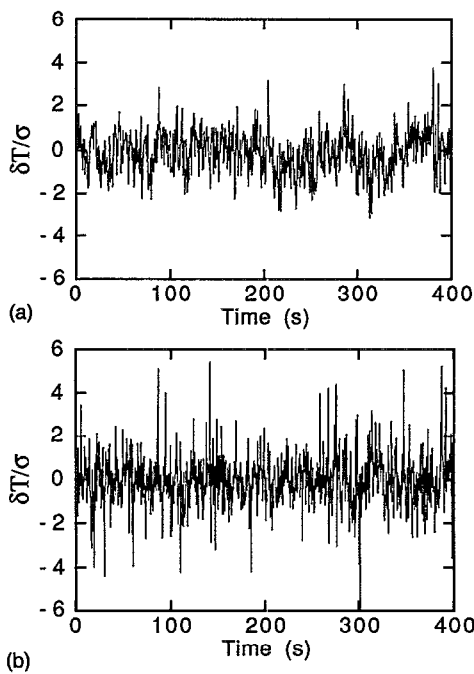
FIG. 7. Temperature time series 5 mm from the grid for (a) $R=300$; (b) $R=1850$. The temperature is expressed in units of the standard deviation. Frequent large excursions from the mean are seen in case (b).
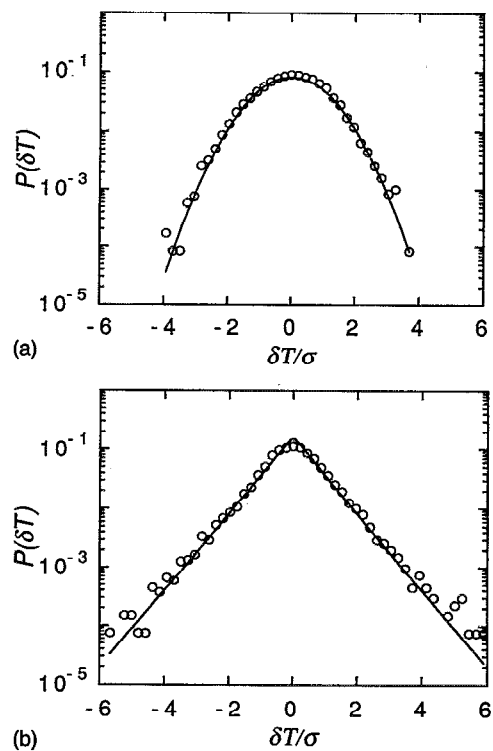

FIG. 8. Temperature probability distributions $P(\delta T)$ corresponding to Fig. 7. (a) $R=300$, (b) $R=1850$. The temperature pdf's have pronounced exponential tails at high R.

The corresponding distributions are shown in Fig. 8. The distribution for $R=300$ is quite adequately described by the Gaussian fit. On the other hand, at $R=1850$ the tails are very nearly exponential. The change is quite dramatic: the observed fluctuations at $\delta T/\sigma=4$ are more probable than those predicted by a Gaussian distribution (with the same variance as that of the data) by a factor of 13. The inverse decay constant γ^{-1} of the exponential is easily seen to be roughly consistent with the value $\beta\xi_V$ predicted in Ref. 11, where β is the local temperature gradient and ξ_v is the velocity correlation length. We were unable to make two-point velocity measurements, but we estimate ξ_v to be approximately equal to the grid hole diameter d. The expected inverse decay constant is then about 0.026 K, in good agreement with the value 0.029 K found experimentally.

The development of the exponential character of the distributions may be summarized by plotting the flatness or kurtosis (ratio of the fourth moment to the square of the second moment) as a function of R, as shown in Fig. 9. This quantity would be 3 for a Gaussian distribution and 6 for a purely exponential distribution. The observed values are consistent with 3 at low R, and rise steadily to the range 5–6 for $R=2000$.

D. Qualifications and limitations

These results must be qualified somewhat: First, clean exponential tails are found only for measurements fairly near the grid and away from the lateral boundaries. (Measurements were typically made about 5 mm below the low-

est extension of the grid.) Farther away (about 15 mm), where the mixing is weaker and the flow is less anisotropic, $P(\delta T)$ is more complex, as shown in Fig. 10(a). The distributions also become asymmetric (not shown) near the lateral boundaries of the cell, with a long tail on one side of the distribution.

More surprisingly, the distributions are often *somewhat* asymmetric even far from the lateral walls, and the degree of asymmetry seems to be unpredictable. An example is shown in Fig. 10(b), which was taken under the same conditions as the more symmetric case presented in
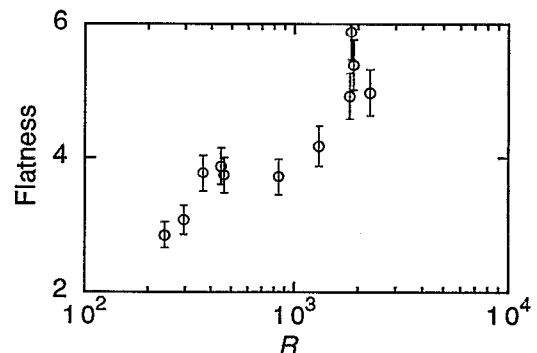

FIG. 9. Flatness or (normalized fourth moment) of the temperature distributions as a function of Reynolds number, based on a few runs at each R. It varies from close to 3 (the Gaussian case) to values above 5 as R is increased.
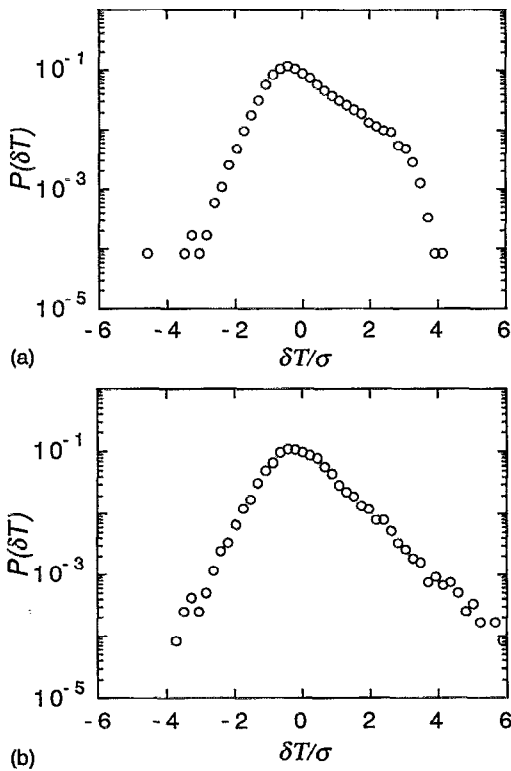
FIG. 10. (a) Temperature distribution farther from the grid (15 mm below its lowest point), where the mixing is weaker, and the distribution more complex. (b) Example of a weakly asymmetric temperature distribution, for the *same* conditions as for Fig. 8(b). The asymmetry is variable and may be a result of very small temperature drifts.

Fig. 8(b). A large number of runs were taken (more than 60), and the mean skewness of the distributions (normalized third moment) is shown for several values of R in Fig. 11, along with error bars indicating the standard deviation of the skewness as an estimate of its variability. It is apparent that the *mean* skewness increases with R, though some individual runs are nearly symmetric.

The relatively large fluctuations in skewness from run to run *may* be due to small temperature drifts. Though the precision of the temperature control (0.01 K) is rather
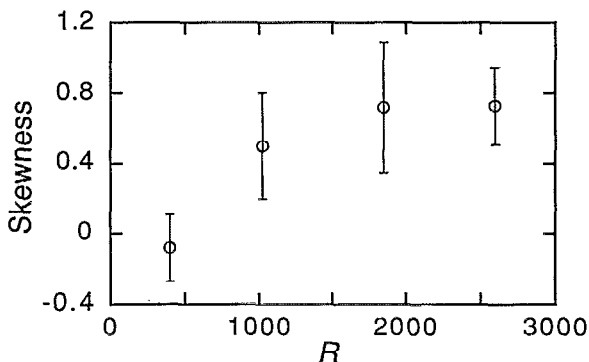

FIG. 11. Mean skewness of the temperature distributions for several values of R, based on a large number of runs, with the standard deviations shown by vertical bars (see text).
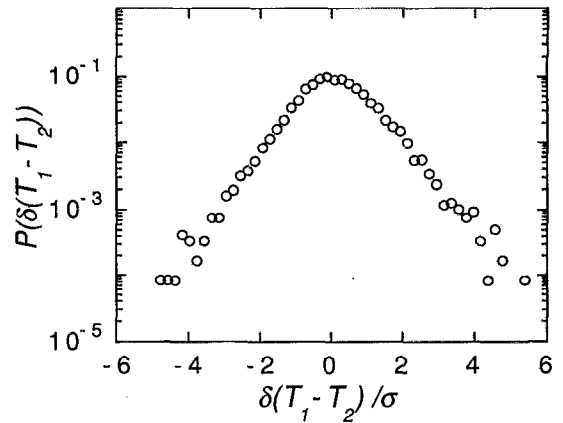

FIG. 12. Temperature *difference* probability distribution at $R=370$ showing non-Gaussian character even at low R.

good for a system transporting heat, the fluctuations are not quite insignificant. For comparison, we note that the mean temperature difference corresponding to 4σ in the temperature pdf's is typically about 0.12 K. Since slow temperature drifts might be expected to distort the temperature distributions, we tried high-pass filtering the data to reduce the effect. However, asymmetry often remained, so in the end we decided it is preferable to use the raw data. Another possible explanation for the skewness is weak large-scale flows, which might arise as a result of increasing instability as R is increased.

Finally, we note that the degree of rounding at the center of distributions is also somewhat variable, again possibly due to unavoidable temperature drifts. This effect may account for the rather large scatter in the flatness plot, Fig. 9.

E. Extensions

The distributions do not depend significantly on the Prandtl number v/κ, where v is the kinematic viscosity and κ the thermal diffusivity. This was confirmed for $R < 500$ by using glycerol–water mixtures. Unfortunately, higher Reynolds numbers were not accessible.

Some experiments were also undertaken for grids with holes (and spacings) scaled up by a factor of 4. The grid may be characterized by the ratio of the hole diameter d to the distance L across the cell parallel to the gradient. When d/L is increased to 0.15 in this way, we find that $P(\delta T)$ is approximately Gaussian for R up to 8000, even though the flow seems to be quite turbulent. The exponential tails do not appear in this case.

Finally, we investigated the probability distributions of temperature *differences* (T_1-T_2) between two probes as an approximation to the temperature *gradient*. If the spacing is less than the thermal correlation length ξ_T, then $P[\delta(T_1-T_2)]$ tends to have extended tails even for rather low R. An example of this behavior is shown in Fig. 12, for probes spaced 6 mm apart at $R=370$. This behavior is not surprising in view of previous work on the non-Gaussian behavior of gradients. If the spacing between the two

probes is increased, then their fluctuations are nearly uncorrelated, and the distribution predictably approaches a Gaussian.

V. DISCUSSION AND CONCLUSION

As we reported in Ref. 20, clear evidence is found for exponential tails in the probability distributions $P(\delta T)$ of the temperature fluctuations for strong mixing, and Gaussian behavior for weaker mixing (Fig. 8). In some cases, the exponential tails extend nearly to the center of the distribution, as indicated by values of the flatness well over 5. This behavior was not anticipated theoretically.

The exponential distributions probably cannot be ascribed to non-Gaussian velocity fluctuations. At the upper end of our range of Reynolds numbers, the velocity distributions are not far from Gaussian, and the velocity spectra are typical of strong turbulence. However, the anisotropy of the flow, caused by the vertical jets, could be a factor in accounting for the thermal statistics.

We have also noted that the distributions $P(\delta T)$ are often asymmetric, but that the fluctuations in the skewness are large from run to run. While we tend to view the asymmetry as evidence either of very small temperature drifts or of weak large-scale flows, it *could* be related to the mechanism proposed by Thoroddsen and Van Atta,[23] who noted skewness in the distributions of *gradients* $P(\partial T/\partial z)$, where z is parallel to the mean temperature gradient in their experiment.

The skewness could affect the flatness measurements to a limited extent. A skewness of 0.6 (the mean value over many runs at $R=2000$) would change the flatness of a perfect exponential distribution from 6 to about 7. While this effect is quantitatively significant, it is not so large as to be the primary factor in the clear trend toward larger flatness as R is increased. In constructing Fig. 9, distributions with skewness larger than 0.5 were excluded to minimize this effect.

Jayesh and Warhaft[21,22] found similar behavior (exponential tails at sufficiently high Reynolds number) for temperature fluctuations in the turbulence behind a grid in a wind tunnel, with an applied cross-stream temperature gradient. They determined both the velocity statistics and the passive scalar statistics, and noted that exponential tails occur when the local Reynolds number based on the Kolmogorov scale exceeds 70. For our experiment, the corresponding grid Reynolds number would be about 100 [based on the rms horizontal velocity rather than the maximum vertical velocity as in Eq. (1)]. Therefore, the two experiments seem compatible, and the exponential tails found for the scalar distributions when there is a mean gradient probably have the same origin.

We did not examine probability distributions in the absence of a mean gradient; Jayesh and Warhaft found Gaussian behavior in that case. They also found that the scalar dissipation rate, proportional to the mean square spatial derivative of the temperature fluctuations, is high for the large fluctuations that are responsible for the exponential tails. It would be interesting to examine the relationship between the pdf and the conditional expectations

of time derivatives of the signal, as pointed out by Pope and Ching.[18] Unfortunately, our sampling rate was not sufficient to allow this comparison; it would be worthwhile to obtain new data for this purpose.

Our measurements [Fig. 3(b)] of the eddy diffusivity D^* for heat, a bulk property, revealed a well-defined transition region near $R=1000$ where the jets through the holes in the grid become strongly turbulent. On the other hand, the nondimensional total heat flux, the Nusselt number N of Fig. 3(a), does *not* show such a transition because it is determined essentially by the boundary layers at the ends of the cell. Jayesh and Warhaft noted that the onset of exponential tails seems to coincide with the value $N=31$ in several different flows. However, we think that this could be an accident in the case of our work, since N is not a bulk property.

It is interesting to speculate as to why the effective diffusivity of dye (Fig. 4) is generally lower than that for heat. One might imagine that the higher thermal diffusivity produces a larger effective transport because heat is more easily transported across separatrices in the flow field. On the other hand, the methods used for these two types of transport measurements are sufficiently different that further work would be required before such a conclusion could be prudently drawn. We note that molecular diffusivity appears to play a role in mixing even at Reynolds numbers considerably higher than those in the present experiments.[24]

We conclude by noting that a clear understanding is still lacking of the precise circumstances under which strong deviations from Gaussian statistics for the scalar distribution should be expected. In a future publication, we will report analogous measurements for steady gradients of passive molecular contaminants, to extend the work on thermal fluctuations contained in this paper.

Note added in proof. Shraiman and Siggia[25] recently computed the pdf using path integral methods. A single scale random velocity field was found sufficient to generate exponential tails as a result of fluctuations in the strain enhanced mixing. Kimura and Kraichnan[26] explored several mechanisms for generating non-Gaussian fluctuations, including one that depends on preferential diffusion in fluid regions that have been highly strained.

2262   Phys. Fluids A, Vol. 5, No. 9, September 1993

Lane *et al.*   2262

[1] M. Avellaneda and A. Majda, "Mathematical models with exact renormalization for turbulent transport, II: Fractal interfaces, non-Gaussian statistics and the sweeping effect," Commun. Math. Phys. **146**, 139 (1992).

[2] S. B. Pope, "PDF methods for turbulent reactive flows," Prog. Energy Combust. Sci. **11**, 119 (1985).

[3] H. Chen, S. Chen, and R. H. Kraichnan, "Probability distribution of a stochastically advected scalar field," Phys. Rev. Lett. **63**, 2657 (1989).

[4] B. Castaing, G. Gunaratne, F. Heslot, L. Kadanoff, A. Libchaber, S. Thomae, X.-Z. Wu, S. Zaleski, and G. Zanetti, "Scaling of hard thermal turbulence in Rayleigh–Bénard convection," J. Fluid Mech. **204**, 1 (1989).

[5] M. Sano, X. -Z. Wu, and A. Libchaber, "Turbulence in helium gas free convection," Phys. Rev. A. **40**, 6421 (1989).

[6] T. H. Solomon and J. P. Gollub, "Thermal boundary layers and heat flux in turbulent convection: the role of recirculating flows," Phys. Rev. A. **43**, 6683 (1991).

[7] C. W. Van Atta and W. Y. Chen, "Structure functions of turbulence in the atmospheric boundary layer over the ocean," J. Fluid Mech. **44**, 145 (1970).

[8] R. Antonia, E. Hopfinger, Y. Gagne, and F. Anselmet, "Temperature structure functions in turbulent shear flows," Phys. Rev. A **30**, 2704 (1984).

[9] P. Kailasnath, K. R. Sreenivasan, and G. Stolovitzky, "Probability density of velocity increments in turbulent flows," Phys. Rev. Lett. **68**, 2766 (1992).

[10] B. Castaing, Y. Gagne, and E. J. Hopfinger, "Velocity probability density functions of high Reynolds number turbulence," Physica D **46**, 177 (1990).

[11] A. Pumir, B. Shraiman, and E. D. Siggia, "Exponential tails and random advection," Phys. Rev. Lett. **66**, 2984 (1991).

[12] A. R. Kerstein, "Linear eddy modeling of turbulent transport, Part 6: Microstructure of diffusive scalar mixing fields," J. Fluid Mech. **231**, 361 (1991).

[13] M. Holzer and A. Pumir, "Simple models of non-Gaussian statistics for a turbulently advected passive scalar" Phys. Rev. E **47**, 202 (1993).

[14] O. Métais and M. Lesieur, "Spectral large-eddy simulation of isotropic and stably-stratified turbulence," J. Fluid Mech. **239**, 157 (1992).

[15] V. Eswaran and S. B. Pope, "Direct numerical simulations of the turbulent mixing of a passive scalar," Phys. Fluids **31**, 506 (1988).

[16] E. S. C. Ching, and Y. Tu, "Passive scalar fluctuations with and without a mean gradient: a numerical study" (to be published).

[17] Y. G. Sinai and V. Yakhot, "Limiting probability distributions of a passive scalar in a random velocity field," Phys. Rev. Lett. **63**, 1962 (1989).

[18] S. B. Pope and E. S. C. Ching, "Stationary probability density functions in turbulence" Phys. Fluids A (in press).

[19] E. S. C. Ching, "Probability densities of turbulent temperature fluctuations" Phys. Rev. Lett. **70**, 283 (1993).

[20] J. P. Gollub, J. Clarke, M. Gharib, B. Lane, and O. N. Mesquita, "Fluctuations and transport in a stirred fluid with a mean gradient," Phys. Rev. Lett. **67**, 3507 (1991).

[21] Jayesh and Z. Warhaft, "Probability distribution of a passive scalar in grid-generated turbulence," Phys. Rev. Lett. **67**, 3503 (1991).

[22] Jayesh and Z. Warhaft, "Probability distribution, conditional dissipation, and transport of passive temperature fluctuations in grid-generated turbulence," Phys. Fluids A **4**, 2292 (1992).

[23] S. T. Thoroddsen and C. W. V. Atta, "Exponential tails and skewness of density-gradient probability density functions in stably stratified turbulence," J. Fluid Mech. **244**, 547 (1992).

[24] M. M. Koochesfahani and P. E. Dimotakis, "Mixing and chemical reactions in a turbulent liquid mixing layer," J. Fluid Mech. **170**, 83 (1986); P. L. Miller and P. E. Dimotakis, "Reynolds number dependence of scalar fluctuations in a high Schmidt number turbulent jet," Phys. Fluids A **3**, 1156 (1991).

[25] B. I. Shraiman and E. D. Siggia, "Lagrangian path integrals and fluctuations in random flow" (to be published).

[26] Y. Kimura and R. H. Kraichnan, "Statistics of an advected passive scalar," Phys. Fluids A **5**, 2264 (1993).